

Anatomical Characterization of Subcortical Descending Projections to the Inferior Colliculus in Mouse

Mili B. Patel,^{1,2} Stacy Sons,¹ Georgiy Yuditsev,³ Alexandria M.H. Lesicko,³ Luye Yang,¹ Gehad A. Taha,¹ Scott M. Pierce,¹ and Daniel A. Llano^{1,3*}

¹Department of Molecular and Integrative Physiology, University of Illinois at Urbana-Champaign, Urbana, Illinois, USA

²Department of Molecular and Cellular Biology, Harvard University, Cambridge, Massachusetts, USA

³Neuroscience Program, University of Illinois at Urbana-Champaign, Urbana, Illinois, USA

Descending projections from the thalamus and related structures to the midbrain are evolutionarily highly conserved. However, the basic organization of this auditory thalamotectal pathway has not yet been characterized. The purpose of this study was to obtain a better understanding of the anatomical and neurochemical features of this pathway. Analysis of the distributions of retrogradely labeled cells after focal injections of retrograde tracer into the inferior colliculus (IC) of the mouse revealed that most of the subcortical descending projections originated in the brachium of the IC and the paralamina portions of the auditory thalamus. In addition, the vast majority of thalamotectal cells were found to be negative for the calcium-binding proteins calbindin, parvalbumin, or calretinin. Using two different

strains of GAD-GFP mice, as well as immunostaining for GABA, we found that a subset of neurons in the brachium of the IC is GABAergic, suggesting that part of this descending pathway is inhibitory. Finally, dual retrograde injections into the IC and amygdala plus corpus striatum as well into the IC and auditory cortex did not reveal any double labeling. These data suggest that the thalamocollicular pathway comprises a unique population of thalamic neurons that do not contain typical calcium-binding proteins and do not project to other paralamina thalamic forebrain targets, and that a previously undescribed descending GABAergic pathway emanates from the brachium of the IC. *J. Comp. Neurol.* 525:885–900, 2017.

© 2016 Wiley Periodicals, Inc.

INDEXING TERMS: thalamus; colliculus; GABA; thalamotectal; thalamocollicular; RRID:IMSR_JAX:007677; RRID:SCR_013286; RRID:AB_477329; RRID:AB_476894; RRID:AB_2619710; RRID:AB_2278725; RRID:AB_476667; RRID:SCR_014432; RRID:SCR_003070; RRID:SCR_014235; RRID:SCR_001775

The inferior colliculus (IC) is a major integration site in the auditory system, and the filter properties of IC neurons are modifiable by manipulations of descending inputs and behavioral context (Yan and Suga, 1998; Ma and Suga, 2001; Malone and Semple, 2001; Yan and Ehret, 2001, 2002; Yan et al., 2005; Metzger et al., 2006; Malmierca et al., 2009). Most previous work on descending control of the IC has been focused on the massive set of projections from the auditory cortex (AC) to the IC (reviewed in Suga, 2008; Bajo and King, 2011; Stebbings et al., 2014). However, additional descending projections to the IC also arise from subcortical structures. For example, several anatomical studies have described projections to the IC that originate in the auditory thalamus, paralamina thalamic nuclei, and brachium of the IC of mice, rats, cats,

gerbils, and monkeys (Adams, 1980; Kuwabara and Zook, 2000; Senatorov and Hu, 2002; Winer et al., 2002; Kuwabara, 2012). These projections target nonprimary parts of the IC (the lateral cortex [LC] and dorsal cortex [DC]), emanate from nonprimary auditory thalamic regions (the medial division of medial geniculate body, supragenulate nucleus, peripeduncular nucleus, and paralamina nuclei) and branch to lower

Grant sponsor: National Institutes of Health (NIH); Grant numbers: DC012125 and DC013073.

*CORRESPONDENCE TO: D.A. Llano, Department of Molecular and Integrative Physiology, 2355 Beckman Institute, University of Illinois at Urbana-Champaign, Urbana, IL 61810. E-mail: d-llano@illinois.edu

Received January 11, 2016; Revised July 29, 2016;

Accepted August 1, 2016.

DOI 10.1002/cne.24106

Published online October 21, 2016 in Wiley Online Library (wileyonlinelibrary.com)

© 2016 Wiley Periodicals, Inc.

brainstem structures. It is not yet known whether these subcortically derived projections to the IC contribute to previously described modifications of IC tuning properties after AC stimulation, although it should be noted that the sources of thalamotectal projections are heavily innervated by the AC (Llano and Sherman, 2008; Mellott et al., 2014).

Previous work in the auditory system of nonmammalian species as well as work from the visual system suggests that the thalamotectal pathway is highly conserved. The dominant descending projection to the frog auditory midbrain is from the posterior thalamus (Feng and Lin, 1991), which may play a role in motivational aspects of phonotaxis (Endepols et al., 2003). The frog thalamotectal pathway may also have an inhibitory component, based on intra- and extracellular recordings in the frog midbrain after thalamic stimulation (Endepols and Walkowiak, 1999, 2001; Ponnath and Farris, 2014). The visual tectum also receives subcortical descending input from the thalamus in turtles (Kenigfest and Belekova, 2009), pretectal and thalamic areas in frog (Ingle, 1973; Trachtenberg and Ingle, 1974; Chapman and Debski, 1995; Li et al., 2005) and rat, at least part of which in all three species is inhibitory (Ingle, 1973; Born and Schmidt, 2004; Li et al., 2005; Kenigfest and Belekova, 2009).

Little is known about the mammalian auditory thalamotectal pathway. The regions of the thalamus containing cells that project to the IC comprise a heterogeneous population of cells with a range of soma sizes, and have neurons with both stellate and elongated morphologies (Senatorov and Hu, 2002; Winer et al., 2002; Smith et al., 2006). These regions of the thalamus generally stain positively for the calcium-binding proteins calbindin or calretinin (Cruikshank et al., 2001; Lu et al., 2009), although it is not yet known which, if any, of these calcium-binding proteins are found in thalamotectal cells. The presence or absence of such calcium-binding proteins has been an integral part of schemes to parse thalamic nuclei (Jones, 2001), and therefore may have functional implications. In addition, the regions of the thalamus populated by thalamotectal cells project to regions outside of the auditory system, such as the basal ganglia and amygdala (Takada et al., 1985; Clugnet et al., 1990; Bordi and LeDoux, 1994). It is not currently known if the same populations of thalamic cells that project to the IC also project to the basal ganglia or amygdala. It is also not known which of these thalamic and related nuclei project to which subnuclei of the IC. Therefore, in the current report we examine: 1) the distribution of thalamic neurons that project to subnuclei of the IC; 2) the presence or absence of staining for the various calcium-binding

proteins in these neurons; 3) whether a component of this pathway is inhibitory; and 4) whether thalamotectal projections are branches of thalamic neurons that project to other forebrain structures, such as the basal ganglia, amygdala, or AC. Earlier versions of this work have been presented in abstract and proceedings form (Patel et al., 2015a,b). For ease of exposition, we will refer to projections to the IC from the thalamus, peripeduncular areas and brachium of the IC as “thalamotectal,” recognizing that not all of these projections come from the thalamus. Specific parsing of this heterogeneous pathway will be done as appropriate in the text.

MATERIALS AND METHODS

Adult (60-day) mice of both sexes were used for this study. As denoted in the text, either Balb/c mice, or mice expressing green fluorescent protein (GFP) in neurons expressing glutamic acid decarboxylase (GAD) were used. Two strains of GAD-GFP mice were used: one commercially available from Jackson Laboratories (Bar Harbor, ME; RRID:IMSR_JAX:007677; Chattopadhyaya et al., 2004) and an additional strain developed and shared by permission from Dr. Yuchio Yanagawa at Gunma University and obtained from Dr. Douglas Oliver at the University of Connecticut (Storrs, CT) (Tamamaki et al., 2003). This mouse is on a Swiss Webster background. All surgical procedures were approved by the Institutional Animal Care and Use Committee at the University of Illinois at Urbana-Champaign, and animals were housed in animal care facilities approved by the American Association for Accreditation of Laboratory Animal Care (AAALAC). Every attempt was made to minimize the number of animals used and to reduce suffering at all stages of the study.

Tracer injections

Mice were anesthetized with ketamine hydrochloride (100 mg/kg) and xylazine (3 mg/kg) injected intraperitoneally and placed in a stereotaxic apparatus. Aseptic conditions were maintained throughout the surgery. Supplements of anesthesia were administered when needed, as determined by response to toe pinch. Injection targets were localized using stereotaxic coordinates (Allen Reference Atlas, RRID:SCR_013286) and the penetration of specific targets were later confirmed using cyto- and chemoarchitectural criteria (see below). Fluorogold (Fluorochrome, Denver, CO) was deposited either using a small piece of gelfoam soaked in tracer, or using microinjections targeted to LC, DC, or central nucleus of the inferior colliculus (CNIC). For microinjections, ~5–10 μ L of tracer was filled into a glass

TABLE 1.
Antibody Information

Antibody name	Structure of immunogen	Manufacturing info	Concentration used
Anti calbindin	Bovine kidney calbindin-D	Sigma Aldrich; C9848; RRI-D:AB_476894; mouse; monoclonal	1:500
Anti calretinin	Recombinant human calretinin containing a 6-his tag at the N-terminal	Swant; CR 7697; RRID: AB_2619710; rabbit; polyclonal	1:500
Anti parvalbumin	Frog muscle parvalbumin	Sigma Aldrich; RRID:AB_477329; P3088; mouse; monoclonal	1:500
Anti-GABA	GABA conjugated to bovine serum albumin	Sigma Aldrich; A0310; RRI-D:AB_476667; mouse; monoclonal	1:500
Anti GAD67	Recombinant GAD67 protein	EMD Millipore; MAB5406; RRI-D:AB_2278725; mouse; monoclonal	1:500
Anti-CTB	Cholera toxin subunit B	List Biological Laboratories, Inc, 703; AB_10013220; goat; polyclonal	1:2000
AlexaFluor 568 goat antimouse	IgG heavy chains and all classes of immunoglobulin light chains from mouse	Life Technologies; A-11004; RRI-D:AB_2534072; goat; polyclonal	1:100
AlexaFluor 568 goat antirabbit	IgG heavy chains and all classes of immunoglobulin light chains from rabbit	Life Technologies; A-11036; RRI-D:AB_10563566; goat; polyclonal	1:100
AlexaFluor 568 rabbit antigoat	IgG heavy chains and all classes of immunoglobulin light chains from goat	Life Technologies; A-11079; RRI-D:AB_10376028; rabbit; polyclonal	1:100

micropipette that had a tip diameter of 1–3 μm . Positive current of 5 μA was applied over a duration of 10–15 minutes using a repeat cycle of 7 seconds on/off. Negative current of 5–10 μA was pulsed using the same repeat cycle while the electrode passed through nontarget zones. The electrode remained in place for 5–10 minutes after each injection to minimize tracking of tracer up the electrode path. For other injections, cholera toxin B (List Biological Laboratories, Campbell, CA) or latex microspheres (Lumafuor Retrobeads, Durham, NC) were used. Glass micropipettes with tip diameters of 5–8 μm were used for pressure injections. Tracer was allowed to settle into the tissue for 5–10 minutes in between these increments and at the end before retracting the electrode.

Tissue processing

Animals were allowed to survive for at least 72 hours postinjection and were then deeply anesthetized with ketamine and xylazine injected intraperitoneally and perfused transcardially with 4% paraformaldehyde in phosphate-buffered saline (PBS). The brains were post-fixed overnight in perfusate. Brains were then cryoprotected through placement in an ascending sucrose gradient until saturated with 30% sucrose in PBS. For brains used for reconstruction purposes, fiducials were made around the structure of interest by lowering a 27.5G needle using a stereotaxic device. Brains were then embedded in egg yolk with 0.7 mL glutaraldehyde and 1 g of sucrose. Frozen 40- μm sections were cut using a sliding microtome and stored in PBS (0.1M, pH 7.4 in all instances). After being allowed to

equilibrate in PBS for at least an hour, sections were heated in the microwave for 15 seconds, washed for 30 minutes in PBS containing 0.3% Triton-X (PBT), followed by a 30-minute blocking step in a 3% serum containing PBT solution. Serum used for blocking was of same species the secondary antibody was generated in. Sections were then incubated with corresponding primary antibody overnight in a cold-room. For secondary antibody staining, sections were first washed in PBT 3 times for 10 minutes each. For GABA immunostaining, the steps were identical except that 1% glutaraldehyde / 4% paraformaldehyde in PBS was used for perfusion. In addition, 5% ethanolamine was added to the PBT. Anti-GABA primary antibody was used at 1:500 dilution. Secondary antibody was diluted in the serum solution used for the primary wash and sections were incubated in this solution for 2 hours at room temperature. At the completion of staining, sections were washed in PBS 3 times for 10 minutes each. Processed sections were mounted on gelatin-coated slides, air-dried, and coverslipped using fluorescence mounting medium (Vectashield, Vector Labs, Burlingame, CA). Clear nail polish was used to keep the coverslip in a fixed position. All slides were stored at 4°C.

Antibody characterization

The parvalbumin monoclonal antibody (Sigma-Aldrich, St. Louis, MO; Cat# P3088 Lot# 122M4774V RRI-D:AB_477329) was generated against purified frog muscle parvalbumin. Per the manufacturer, this antibody does not react with other members of the EF-hand family, such as calmodulin, intestinal calcium-binding

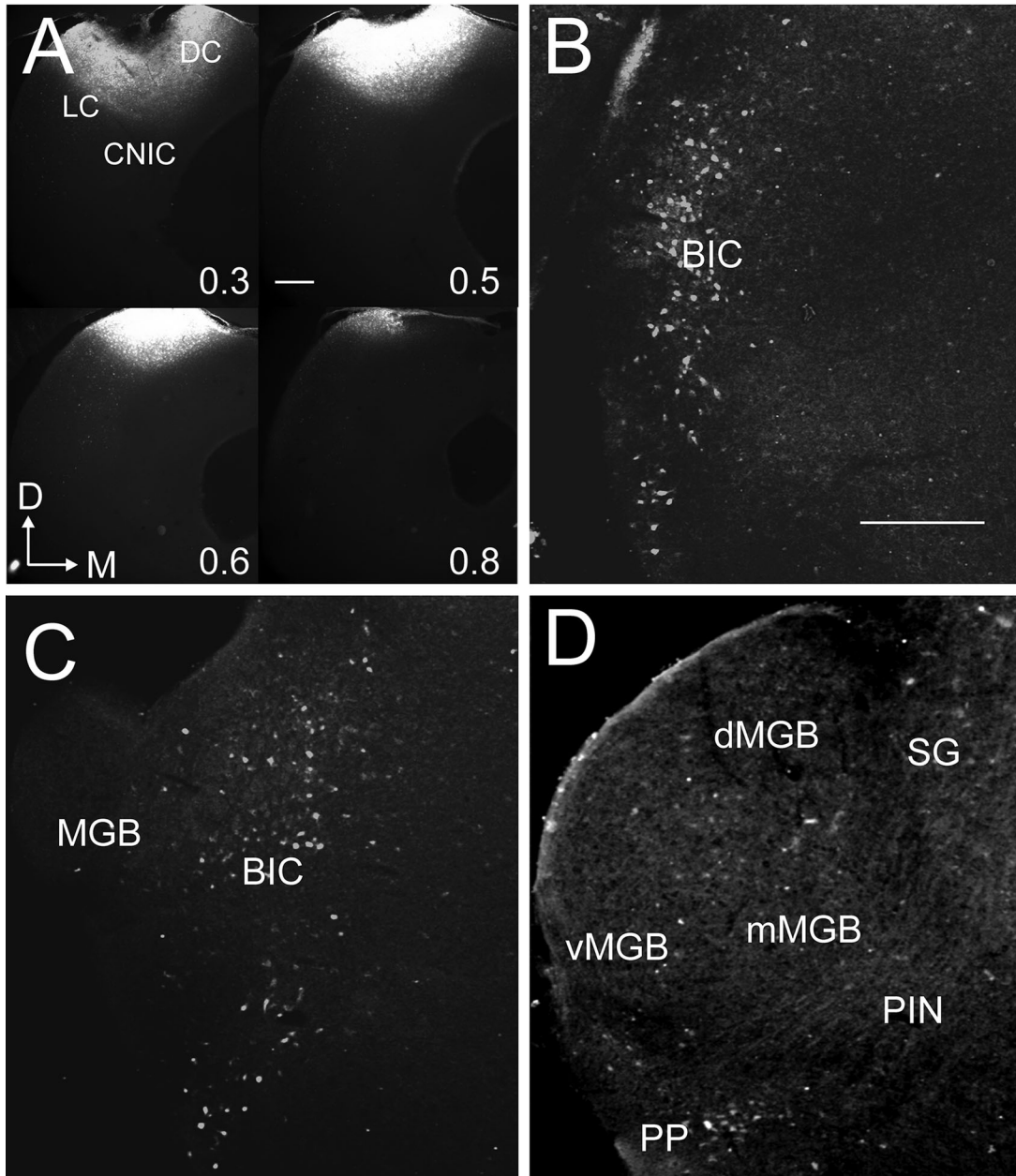


Figure 1. Example of the distribution of cells projecting to the IC from thalamus and adjacent structures. **(A)** Four images from the injection site after deposit of Fluorogold-soaked gelfoam was placed into the IC. Numbers in lower right corner correspond to the caudal-rostal location of the slice (0.0 = most caudal portion of the IC, 1.0 = most rostral portion of the IC). Backlabeled cells are seen in the BIC **(B)** as well as MGB and adjacent structures **(C,D)**. D = dorsal, L = lateral. Scale bar = 250 μ m.

protein, S100A2 (S100L), S100A6 (calcyclin), the α chain of S-100 (i.e., in S-100a and S-100ao), or the β chain (i.e., in S-100a and S-100b). The calbindin monoclonal antibody (Sigma-Aldrich Cat# C9848 clone CB-955 Lot# 063M4760 RRID:AB_476894) was generated against bovine kidney calbindin-D. Per the manufacturer, this antibody does not react with other members of the EF-hand family, such as calbindin-D-9K, calretinin, myosin light chain, parvalbumin, S-100a, S-100b,

S-100A2 (S100L), and S-100A6 (calcyclin). The calretinin polyclonal antibody (Swant, Bellinzona, Switzerland; Cat# CR 7697, Lot# 1893-0114 RRID: AB_2619710) was generated against human calretinin containing a 6-his tag at the N-terminal. Per the manufacturer, this antibody does not react with calbindin D-28k or other known calcium-binding proteins. The manufacturer demonstrates the specificity of this antibody by showing the absence of binding in calretinin knockout mice

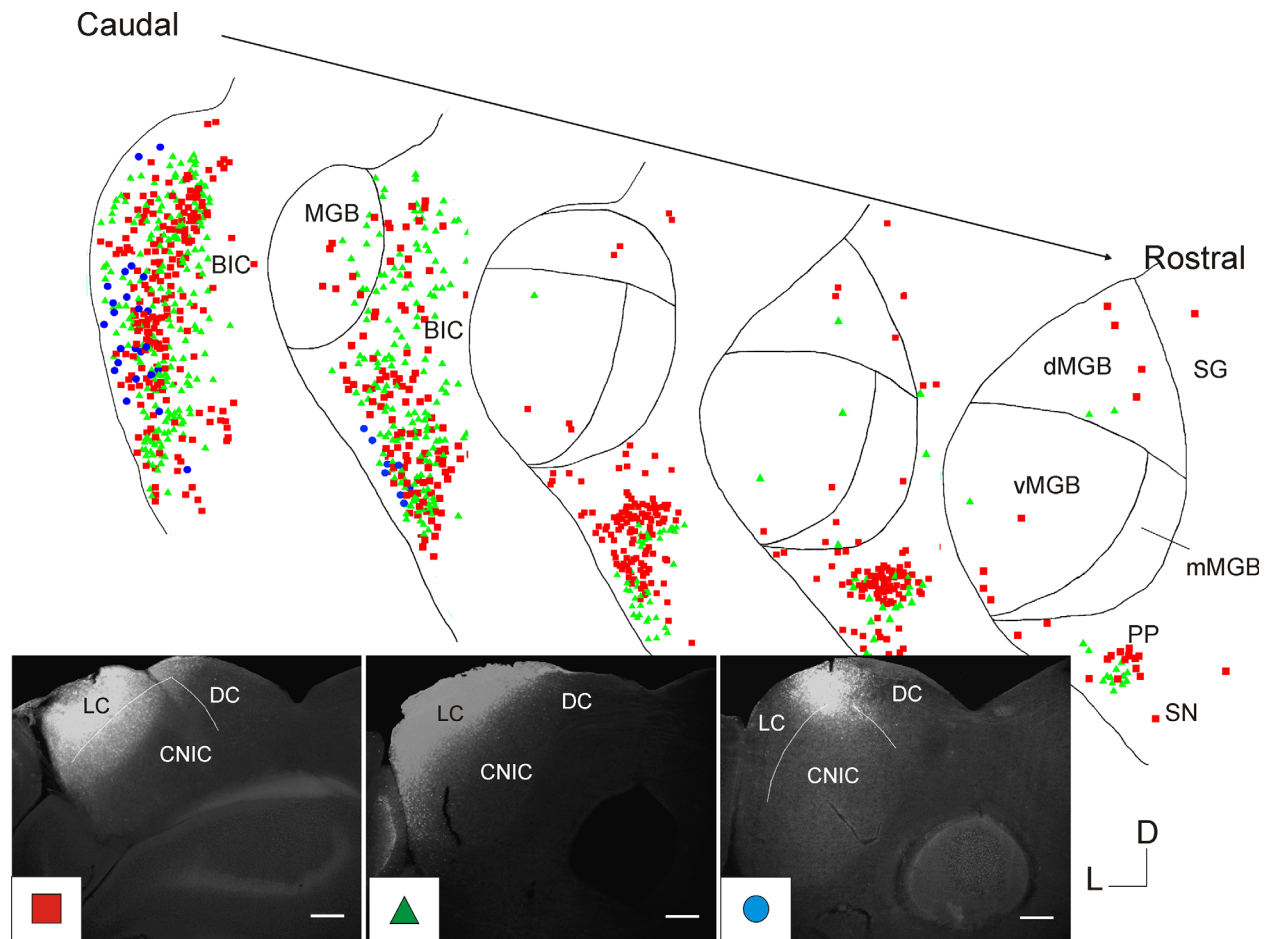


Figure 2. Distribution of backlabeled cells after injection of tracer into LC. Top: Five representative sections from caudal to rostral illustrating the distribution of backlabeled cells from three different animals, color-coded by animal. Intra-MGB borders are not distinguished in the caudalmost section of the MGB (see text for details). Bottom: Injection sites for three different animals. Dotted lines correspond to nuclear borders, when available either via nuclear or GAD staining. Shape and color in bottom left corner of each injection site photo correspond to the backlabeled cells projected onto the drawings above. In all cases, Fluorogold was used to inject. Scale bars = 100 μm .

(http://www.swant.com/pfd/7697_Rabbit_anti_calretinin.pdf). The CTB polyclonal antibody (List Biologicals; Cat# 703, Lot# 7032A8, AB_10013220) was generated against CTB in goat. The anti-GAD antibody (Millipore, Bedford, MA; Cat# MAB5406 Lot# 2390525 RRID:AB_2278725) was generated against recombinant GAD67 protein. Per the manufacturer, the antibody “Reacts with the 67kDa isoform of Glutamate Decarboxylase (GAD67) of rat, mouse and human origins, other species not yet tested. No detectable cross reactivity with GAD65 by Western blot on rat brain lysate when compared to blot probed with AB1511 that reacts with both GAD65 & GAD67.” The anti-GABA antibody (Sigma-Aldrich; Cat# A0310 Lot# 074M4801V RRID:AB_476667) was generated against GABA conjugated to bovine serum albumin. Per the manufacturer, “The antibody does not cross react with

L- α -aminobutyric acid, L-glutamic acid, L-aspartic acid, glycine, δ -aminovaleric acid, L-threonine, L-glutamine, taurine, putrescine, L-alanine and carnosine. However, weak cross-reaction is observed with β -alanine and ϵ -aminocaproic acid.” For all secondary antibodies, we have run controls by eliminating primary antibody and have not seen signal (data not shown). See Table 1 for more information on the antibodies used.

Image processing and analysis

All images were captured using either the Olympus 1X71 fluorescence microscope or the Zeiss LSM 710 confocal microscope. Images were captured using either Q Capture Pro (<http://www.qimaging.com/products/software/qcappro7.php> RRID:SCR_014432) or Zen10 software and processed using ImageJ and

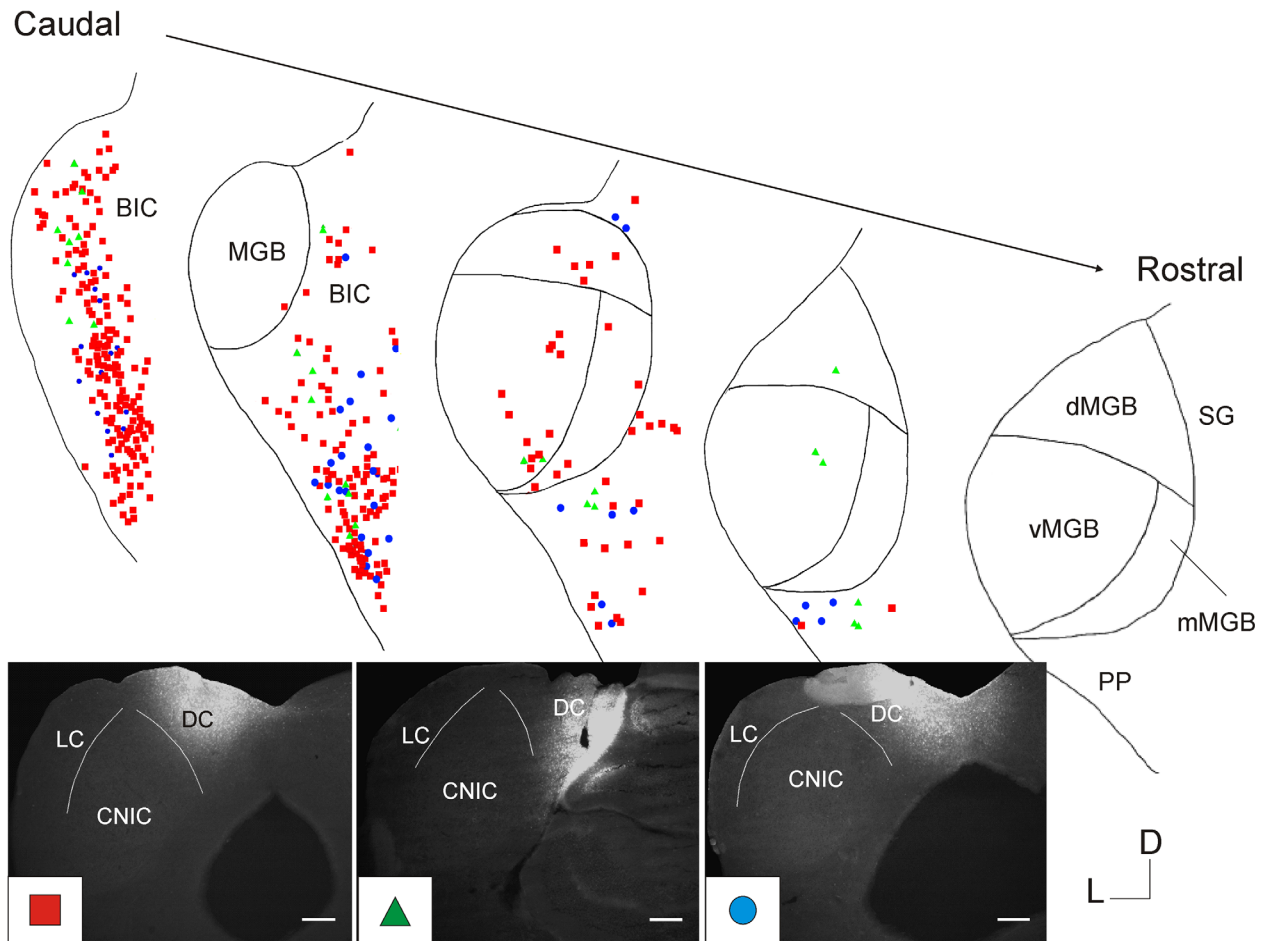


Figure 3. Distribution of backlabeled cells after injection of tracer into DC. The figure is organized in an identical manner as Figure 2.

Adobe Photoshop (San Jose, CA). Scale bars were inserted in ImageJ (<https://imagej.nih.gov/ij/>; RRID:SCR_003070), corresponding false colors were applied to individual images, and then overlays were made in the same program. Photoshop elements 13.0 or Corel Draw (<http://www.coreldraw.com/en/>; RRID:SCR_014235) was used to retouch images in parts surrounding the brain tissue and to adjust brightness, contrast and color balance. NeuroLucida software (<http://www.mfbioscience.com/neuroLucida>; RRID:SCR_001775) was used to create serial section reconstructions to visualize the distributions of thalamotectal cells in thalamus and BIC in three dimensions. Raw images were imported in the software, cells were marked in each section manually, contours were drawn around boundaries of the thalamus, and sections were matched using at least two fiducial markers. For determining calcium-binding protein-positive thalamotectal cells, all labeled cells from the large foam injections were counted in NeuroLucida. Then high-magnification overlays

were used to judge how many of these cells were positive for the corresponding calcium-binding protein. No efforts were made to correct for potential double-counting of cells at the border between sections. This is because the overwhelming majority of backlabeled cells (>90%) were not immunopositive for calcium-binding proteins, and therefore potential cell double-counting would have negligible impact. For determining overlap in thalamotectal cells with thalamocortical, thalamoamygdalar, or thalamostriatal cells, high-magnification images of corresponding regions were manually analyzed. All images were obtained in black and white, and then pseudocolored in magenta or green to provide maximum color contrast that can be distinguished even in the presence of red-green color blindness.

RESULTS

Distributions of thalamotectal cells

Figure 1 demonstrates the general distribution of retrogradely labeled cells in the BIC and thalamus after

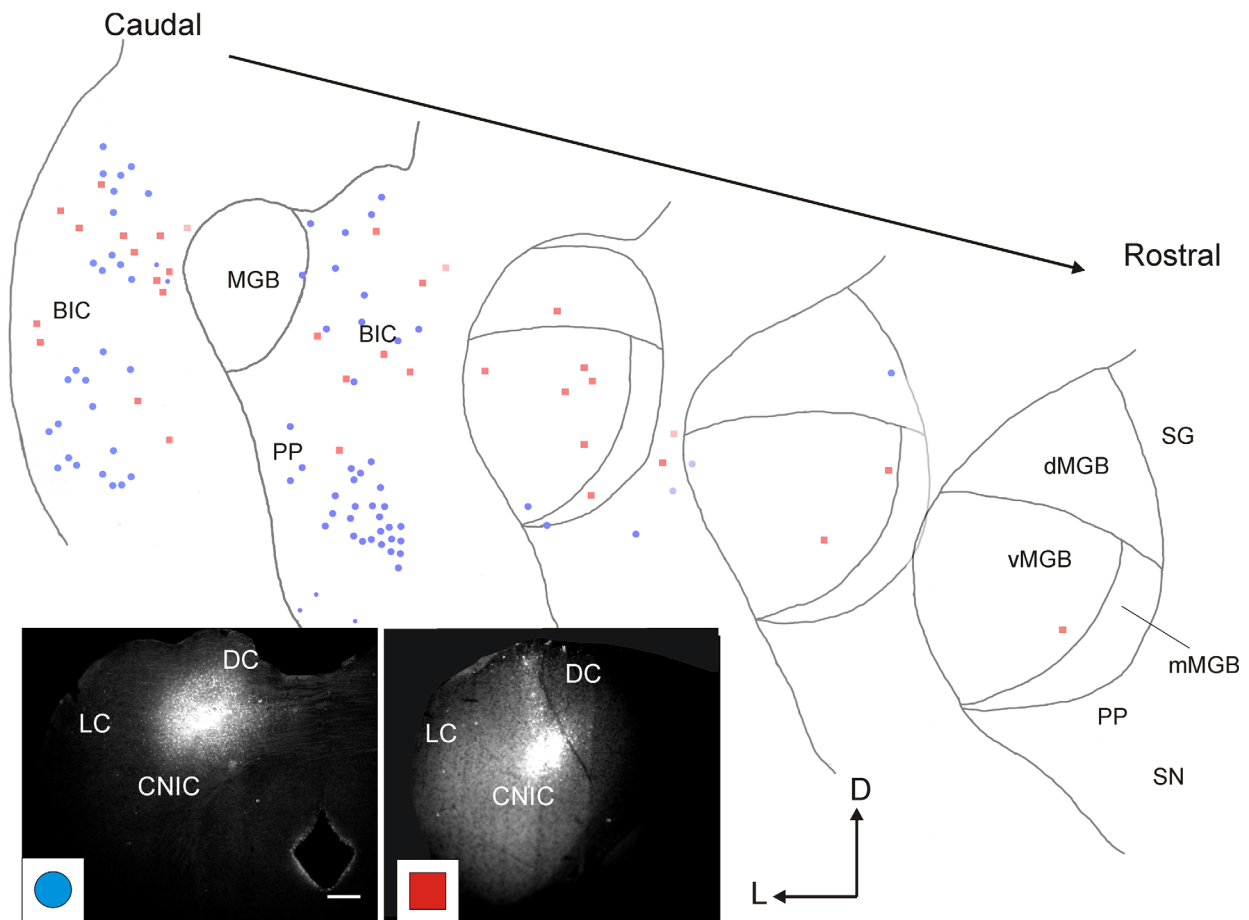


Figure 4. Distribution of backlabeled cells after injection of tracer into CNIC. The figure is organized in an identical manner as Figures 2 and 3, except that only two injection sites are shown.

injection of Fluorogold using soaked gelfoam deposited into the IC, with an injection site that encompasses portions of the three major subdivisions of the IC: LC, DC, and CNIC (Fig. 1A). Similar to previous reports (Senatorov and Hu, 2002; Winer et al., 2002), the bulk of the retrograde label was found in the BIC and the paralamina nuclei of the posterior thalamus: the medial division of the medial geniculate body (mMGB), supra-geniculate nucleus (SG), the posterior intralamina nucleus (PIN), and the peripeduncular nucleus (PP), although some label was observed in the areas of the MGB more traditionally associated with thalamocortical transmission: the ventral division of the MGB (vMGB) and dorsal division of the MGB (dMGB, Fig. 1B–D). Occasional cells were seen in the subparafascicular nucleus, as have been previously described (Nevue et al., 2015), but only with large injections of Fluorogold into the IC.

To determine which portions of the thalamus and nearby structures project to which portions of the IC, small deposits of Fluorogold were iontophoretically

injected into either the LC, DC, or CNIC. Calbindin immunostaining was used to delineate the subnuclei of the MGB and either Nissl staining with Neurotrace or immunostaining with GAD67 was used to delineate the subnuclei of the IC. Such nuclear staining was not done in all animals, and nuclear borders are drawn onto figures when these data were available. Note that similar to Cruikshank et al. (2001), we were unable to delineate MGB subnuclei in the caudal extreme of the MGB, where calbindin immunostaining is uniformly heavy. Previous investigators have determined that this region likely contains portions of both the dMGB and mMGB, based on cytoarchitectural criteria (Winer et al., 1999). Therefore, we have not delineated these nuclei here, and simply label this region “MGB.”

Three injections into the LC are included in this data compilation and the injection sites are color-coded and shown in the inset of Figure 2. As shown, most of the injectate remained in the LC, with some spillage of the red-coded injection site into the CNIC. The resulting

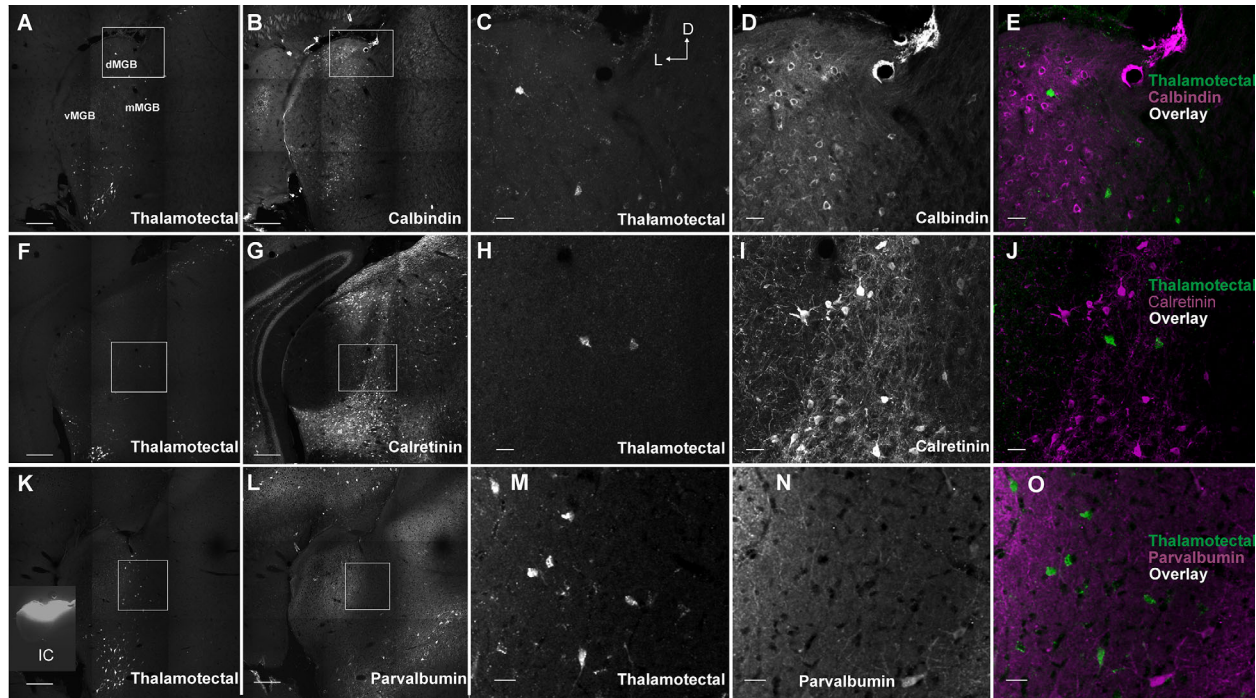


Figure 5. Evaluation of double-labeling of thalamotectal cells with calcium-binding proteins. **(A,B)** Composite 20× photos (nine photos each, arranged 3 × 3) views of backlabeled cells after FG injection into the IC (A) and immunostain for calbindin (B). **(C–E)** Zoomed 20× views showing backlabeled thalamotectal cells (C), calbindin positive cells (D) and an overlay image (E) with thalamotectal cells in green and calbindin cells in magenta, from the square shown in (A). **(F–J)** Similar to A–E, but for calretinin. **(K–O)** Similar to A–E, but for parvalbumin. Inset in bottom left of (K) is the same injection site for all three sets of images. Scale bars = 250 μm in A,B,F,G,K,L; 20 μm in C–E,H–J,M–O.

TABLE 2.

Calcium-Binding Protein Immunopositivity per Total Number of Backlabeled Thalamotectal Cells

	Calbindin	Calretinin	Parvalbumin
dMGB	16/228 (7%)	21/534 (4%)	6/150 (4%)
mMGB	1/155 (1%)	4/456 (1%)	5/63 (8%)
vMGB	0/3	1/1	1/5

N = 8 animals for parvalbumin; *N* = 9 animals for calbindin and calretinin.

distribution is shown in a caudal-to-rostral gradient and shows that: 1) most of the retrogradely labeled cells were in the BIC and the paralamina nuclei of the thalamus with dense innervation from the PP. There were scattered cells in the dMGB and vMGB as well as the substantia nigra. As sectioning proceeded more rostrally in the thalamus, most cells became concentrated into the PP. The smallest injection site (color-coded blue) only labeled cells in the BIC.

Figure 3 shows the distribution of retrogradely labeled cells in the BIC and thalamus after deposit of tracer into the DC. The density of labeling appears sparser than the LC injections, although the injection sites are necessarily

smaller (see inset of Fig. 3). The distribution of labeled cells appears similar to the LC; most retrogradely labeled cells are in the BIC and paralamina nuclei, although there appears to be a cluster of cells in the PP, as described after LC injections (Fig. 2), and scattered labeled cells in the vMGB and dMGB. Small numbers of cells were seen in similar regions contralaterally (BIC, PP, and paralamina nuclei of the posterior thalamus after both LC and DC injections), although the relative proportion of contralateral cells were larger after DC injections (data not shown).

Two CNIC injections were included in this analysis (Fig. 4). Both injection sites were relatively small to limit spillover into other parts of the IC. Similar to the findings of Kuwabara (Kuwabara and Zook, 2000; Kuwabara, 2012), there appears to be very few cells in the BIC or thalamus that project to the CNIC. Most of the backlabeled cells were found in the BIC and caudal portion of the PP. Taken together, the data in Figures 2–4 suggest that, similar to the corticocollicular system (Saldaña et al., 1996; Winer et al., 1998; Bajo et al., 2007; Budinger et al., 2013; Torii et al., 2013), most descending input from the BIC and thalamus appear to target the DC and LC, and most are derived from the BIC, PP

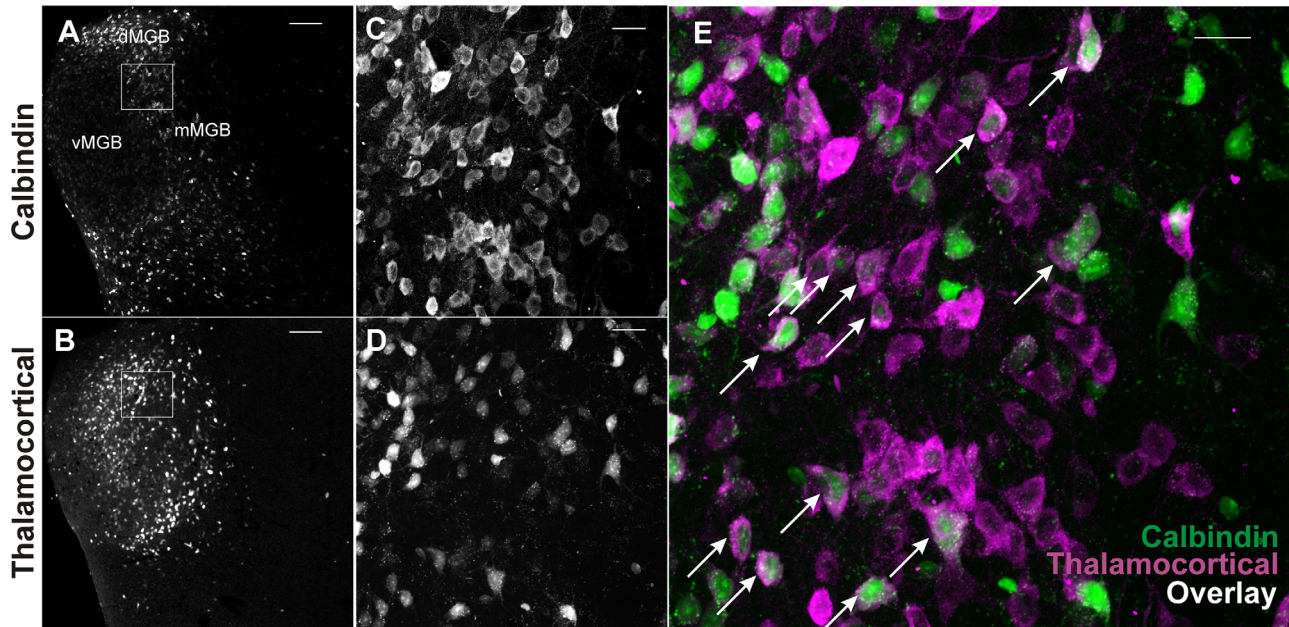


Figure 6. Positive control for combining immunostaining with backlabeling of cells with Fluorogold. **(A,B)** Low-powered images of the MGB after immunostaining for calbindin (A) or placing Fluorogold into the AC (B). **(C)** Higher-power view from square shown in panel A showing calbindin-positive neurons. **(D)** Higher-power view from same field in panel C showing backlabeled thalamocortical cells. **(E)** Overlay image showing multiple double labeled cells (denoted with white arrows). Green = Fluorogold labeled cells. Magenta = calbindin labeled cells. Scale bars = 100 μm in A,B; 30 μm in C-E.

with more limited contributions from the MGB. The small degree of potential spillover of tracer from CNIC to adjacent nuclei may account for some of the apparent projections to the CNIC.

Calcium-binding protein characteristics

To determine which, if any, of the calcium-binding proteins were expressed in thalamic cells backlabeled after IC injection of Fluorogold, large injections (using gelfoam) were made in the mouse IC, followed by immunostaining for parvalbumin, calbindin, or calretinin. Gelfoam was used to achieve saturation of the IC to ensure that negative results were not due to inadequate backlabeling of thalamic cells. We found this approach to produce variable numbers of backlabeled cells, and no attempt was made to normalize the counts per injection site size since findings in all animals were similar. Data were pooled across eight animals for parvalbumin and nine animals for calbindin and calretinin. We note that the majority of backlabeled cells were found in the BIC, consistent with data from the smaller injections described in Figures 2–4. Only the MGB data were analyzed for calcium-binding proteins given the importance of these proteins in parcellation schemes of the thalamus (Jones, 2001). As shown in Figure 5, the overwhelming majority of thalamotectal cells did not stain positively for any of these

three markers. We found that 4.4%, 4.3%, and 2.6% of the backlabeled thalamotectal cells also stained positively for parvalbumin, calbindin, or calretinin, respectively, across 218, 386, and 991 backlabeled cells, respectively. Data were also parsed by subregion (dMGB, vMGB, mMGB) and none of the percentages in the dMGB or mMGB exceeded 10% (Table 2). Too few cells were seen in the vMGB to justify computing the percent of positive cells. As a positive control to ensure that Fluorogold did not interfere with immunostaining, in a separate animal thalamocortical cells were backlabeled using Fluorogold injection into the AC. As shown in Figure 6, as expected, many backlabeled cells, in this case in the dMGB, also stained positively for calbindin.

GABAergic descending projections to the IC

Retrograde tracer was placed into the IC of two different strains of GAD-GFP mice (Tamamaki et al., 2003; Chattopadhyaya et al., 2004). A number of retrogradely labeled cells were found in the BIC that were also GAD+ (Fig. 7C–E). Double-labeled cells were rarely observed in the PP, which also had many GABAergic neurons (Fig. 7F–H). In the MGB, very few GAD+ cells were observed, and these did not backproject to the IC. Data are shown in Figure 7 for the GAD-GFP mouse from Tamamaki et al., but additional

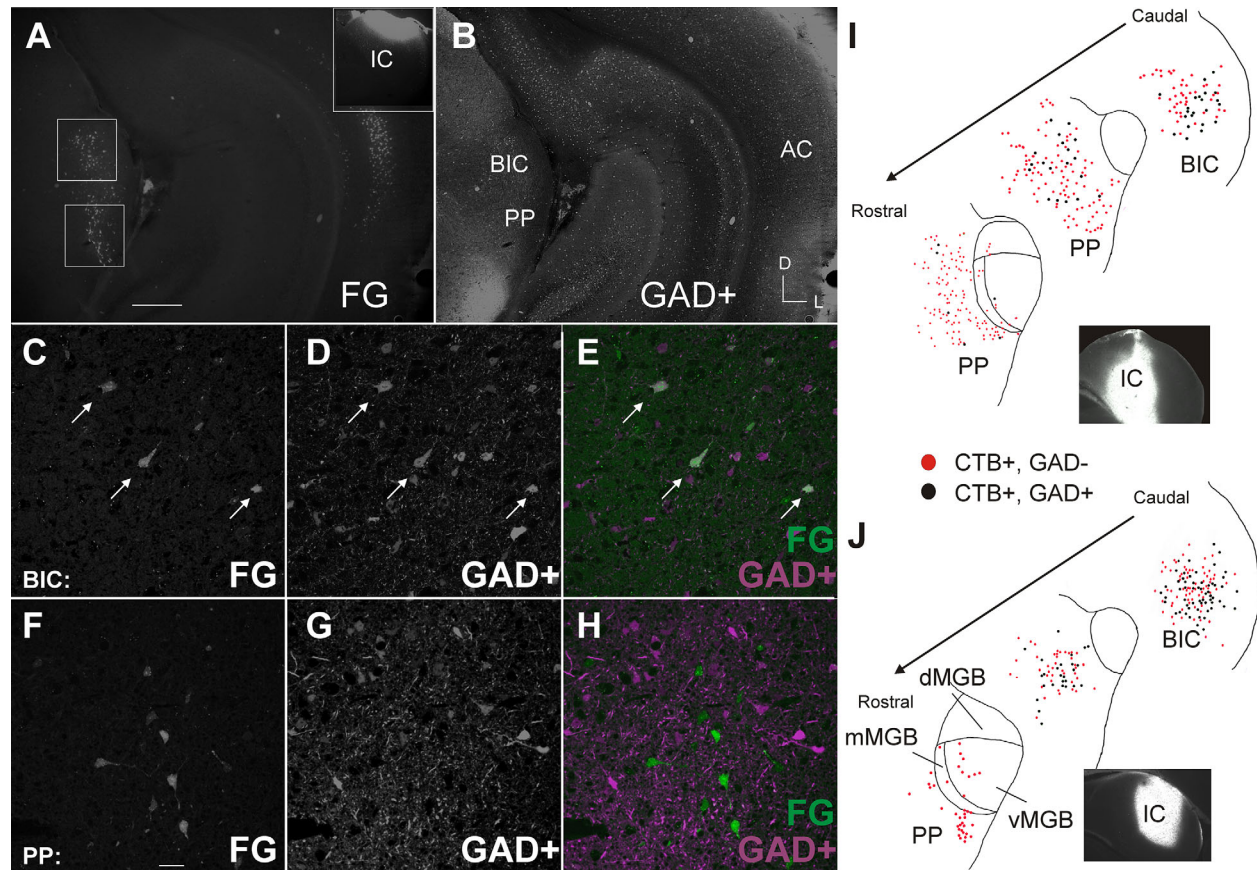


Figure 7. GABAergic cells from the BIC project to the IC. **(A)** Low-power image of backlabeled cells backlabeled after injection of FG into the IC (injection site in inset). Boxes correspond to BIC (upper box) and PP (lower box). **(B)** Same section as **(A)**, immunostained for GAD67+. **(C)** 40 \times confocal image of backlabeled cells in the BIC. **(D)** 40 \times confocal image of GAD + tissue in the BIC. **(E)** Overlay between **(C,D)**. White arrows point to double-labeled cells. **(F)** 40 \times confocal image of backlabeled cells in the PP. **(G)** 40 \times confocal image of GAD + tissue in the PP. **(H)** Overlay between **(F,G)**. No double-labeled cells are seen. **(I,J)** Distributions of backlabeled cells in the posterior thalamus and BIC of two GAD-GFP mice injected with CTB in the IC (injection sites in insets). Backlabeled cells which were either GAD+ (black circles) or GAD- (red circles). Scale bars = 500 μ m in **A**; 20 μ m in **C-H**.

experiments were done with CTB and with a different strain of GAD-GFP mouse (Chattopadhyaya et al., 2004), with similar findings across animals and tracers (data not shown). Two additional mice had injections of CTB into the IC, and the distributions of backlabeled cells in the posterior thalamus and BIC were counted in NeuroLucida and shown in Figure 7I,J. Across these two animals, 260 backlabeled cells were found in the BIC, and 128 (49%) were found to be GAD+, while 2/119 cells in the PP (1.6%) were found to be GAD+ ($P < 0.0001$, chi-square = 81.9, degrees of freedom = 1). GABAergic projections from the BIC to the IC were also observed using immunostaining for GABA. Figure 8 shows backlabeled cells in the BIC after injection of FG into the IC (Fig. 8A). GABA immunostaining reveals a subset of IC projecting neurons in the BIC that are GABAergic (Fig. 8C, arrows for double-labeled cells).

Branching of thalamotectal cells

To determine if thalamotectal projections are branches of thalamic neurons projecting to other regions known to be targets of neurons in the paralamina thalamic nuclei, dual injections of tracers were made into the IC and either the AC ($n = 3$ mice) or a region encompassing the amygdala and corpus striatum ($n = 3$ mice, see Fig. 9A,B,D,E for example injection sites). In all cases, numerous auditory thalamic cells were backlabeled from the AC, IC, or striatum/amygdala region. However, no double-labeled cells were ever observed (see Fig. 9C,F representative high-powered examples from the mMGB after dual backlabeling in AC+IC or amygdala/corpus striatum+IC). Quantification and comparison of the numbers of double-labeled cells was not done since no double-labeling was observed.

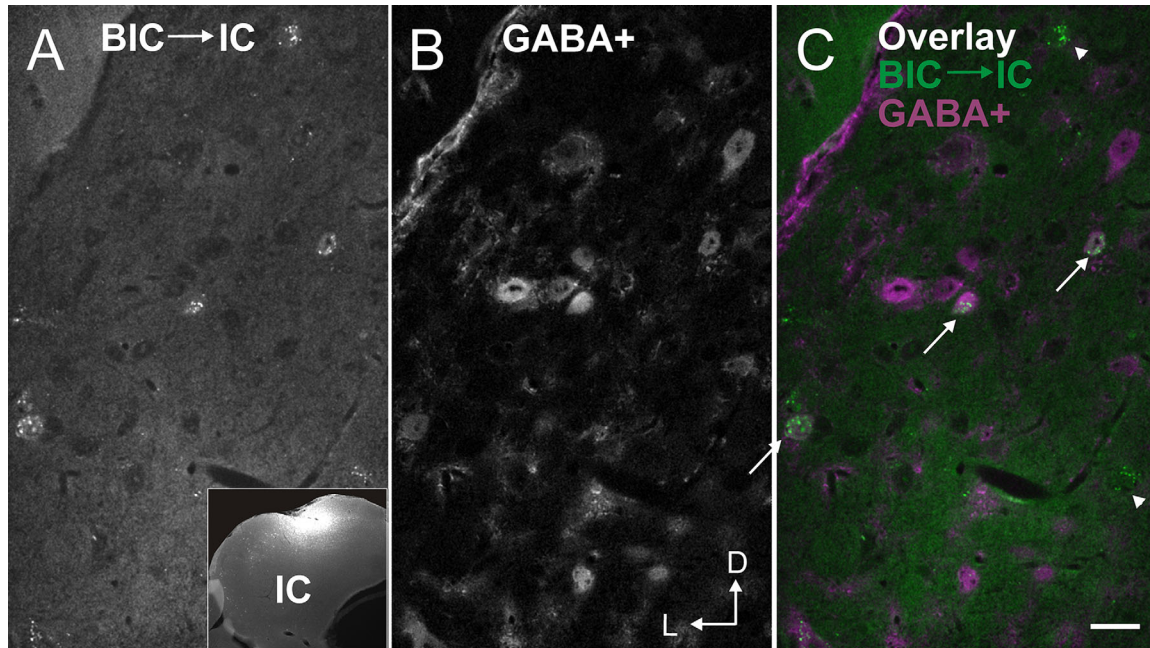


Figure 8. Immunostaining of GABAergic cells from the BIC that project to the IC. **(A)** Backlabeled cells in the BIC after injection of FG into the IC (injection site in inset). **(B)** GABA + cells in the same section of the BIC. **(C)** Overlay between (A,B). Arrows show double-labeled cells. Arrowheads point to backlabeled cells that are negative for GABA. Scale bar = 20 μm .

DISCUSSION

In this study we report that subcortical descending projections to the IC are derived from a number of structures, including the BIC, SG, mMGB, dMGB, vMGB, PIN, and PP. We find that these cells target the DC and LC divisions of the IC and that the overwhelming majority of these cells do not colocalize with any of the classic calcium-binding proteins used previously to parse thalamic nuclei. We also find that these IC-projecting cells do not branch to other known targets of the paralaminar regions of the thalamus: the amygdala/striatal region or AC. Finally, a subset of cells that project from the BIC to the IC appears to be GABAergic. Therefore, the cells described in this report appear to comprise a unique population of cells in the thalamus whose primary projection appears to be towards the sensory periphery and does not share many neurochemical or connectional features with neighboring cells. Technical limitations and potential functional implications are discussed below.

Technical considerations

Several limitations to the approaches employed in this study should be considered when interpreting these results. One limitation has to do with our negative finding of branched thalamic cells, assessed by

the use of dual retrograde tracers. It is possible that branching cells to the IC and AC or amygdala+striatum from the thalamus do in fact exist, but that we failed to observe them because our injection sites were too small or were not placed in the projection zone of each branch (i.e., they were not “matched”). We acknowledge this, and recognize other, more gold standard approaches, such as anterograde filling and directly observing axonal branching obviates these concerns. For the current study, we attempted to compensate for this concern by making relatively large injections in each site. Despite these large injections, we repeatedly saw zero double-labeled cells. Therefore, we interpret these findings to mean that if there are thalamic cells with branches to the IC and amygdala or IC and AC, these comprise a very small population.

Another potential technical concern is that since the characterization of thalamocollicular cells was based purely upon the use of retrograde tracers, it is possible that the tracer injections, in fact, labeled axons passing through the IC en route to other, more caudal, structures. We cannot exclude this possibility, although previous anterograde studies are entirely consistent with the current results. That is, filling thalamotectal cells with biocytin has established that these cells have terminals in the nonprimary parts of the IC and

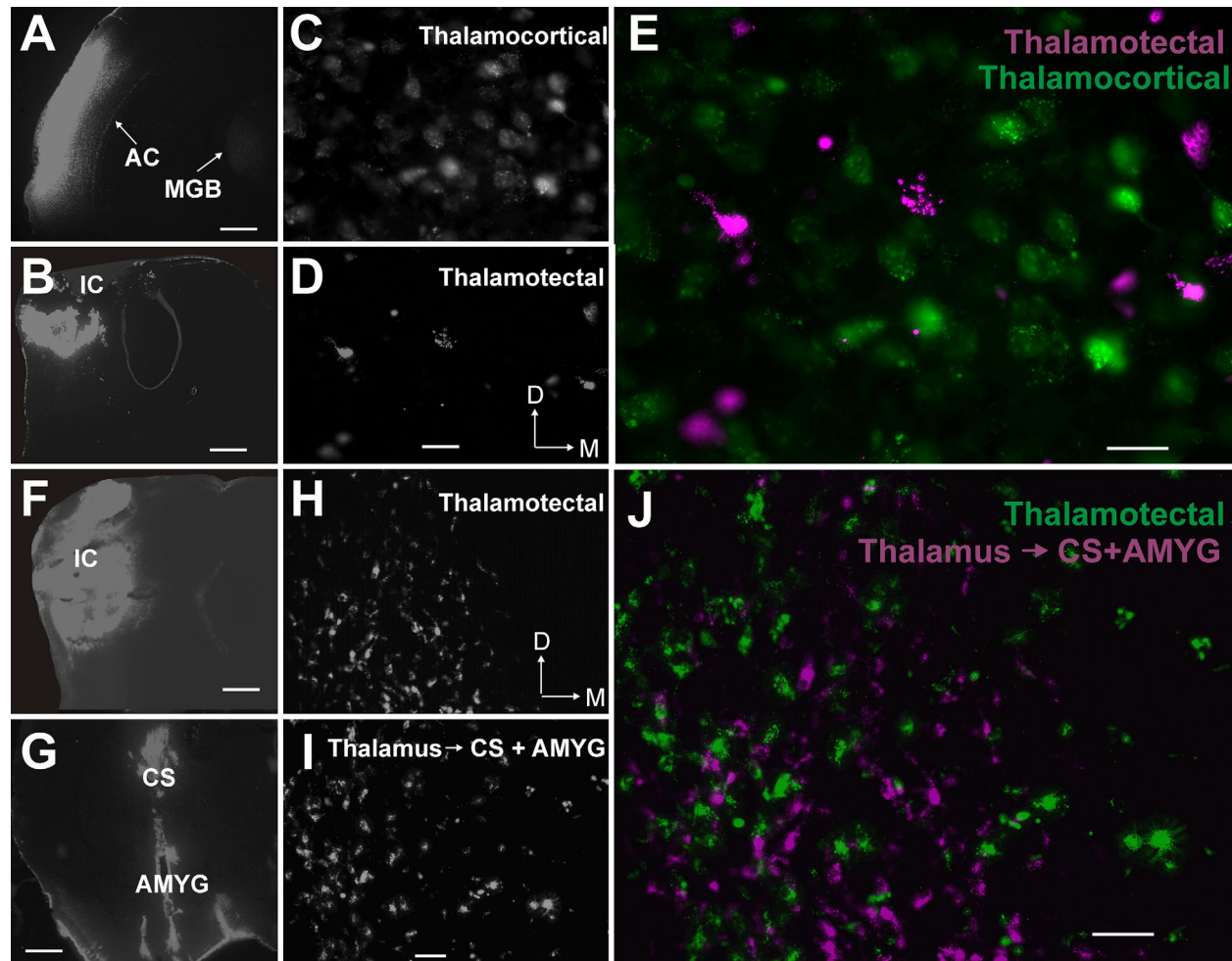


Figure 9. Thalamotectal cells do not project to the AC, amygdala or corpus striatum. **(A)** Injection site of Fluorogold into the AC. Backlabeled cells are seen in the MGB. **(B)** Injection site of Retrobeads into the IC. **(C)** High-powered image from the mMGB showing backlabeled thalamocortical cells. **(D)** High-powered image from the same mMGB field showing backlabeled thalamotectal cells. **(E)** Overlay image from panels C and D showing absence of double-labeled cells. **(F)** Injection site of Retrobeads into the IC, **(G)** Large injection site of Retrobeads encompassing the amygdala (AMYG) and corpus striatum (CS). **(H)** High-powered image from the mMGB showing backlabeled thalamotectal cells. **(I)** High-powered image from the same mMGB field showing backlabeled thalamic cells projecting to the CS and/or the AMYG. **(J)** Overlay image from panels H and I showing absence of double-labeled cells. Scale bars = 25 μ m in C–E; 50 μ m in H–J, 500 μ m in A and G; 250 μ m in B and F.

avoid the CNIC (Kuwabara and Zook, 2000; Kuwabara, 2012).

Finally, it is possible that our use of gelfoam injections to saturate the IC for parts of this study led to undetected leak of tracer into adjacent brain regions, such as the superior colliculus, nonspecifically backlabeling portions of the MGB, and/or shifting the proportions of cells in different thalamic subnuclei. The gelfoam approach was used to saturate the IC with tracer to achieve a maximal number of backlabeled cells, which is particularly important when interpreting negative results (e.g., absence of calcium-binding protein colocalization and absence of branching of thalamotectal cells to forebrain structures). Arguing against

the possibility that nonspecific labeling was seen is the general similarity of the distributions of backlabeled cells observed in our study compared to other studies using different tracers and different injection techniques (Senatorov and Hu, 2002; Winer et al., 2002). Nevertheless, given the known caudal diencephalic projections to the superior colliculus (Edwards et al., 1979; Appell and Behan, 1990; Comoli et al., 2012), there exists a small possibility that some of the thalamotectal projections here target the superior colliculus.

Comparison with previous studies

To our knowledge, there have been only five previous published reports that have examined the projections

to the mammalian IC from the thalamus and related structures (Adams, 1980; Kuwabara and Zook, 2000; Senatorov and Hu, 2002; Winer et al., 2002; Kuwabara, 2012). These studies described projections emanating from the paralaminae thalamic nuclei and BIC and project to the DC and LC of the IC, very similar to the observations in the current report. Further, backlabeled cells in the Winer et al. study showed heterogeneous morphologies, distinct from the typical bitufted morphology seen in thalamocortical cells. Thus, many of these cells resemble paralaminae cells adjacent to the auditory thalamus examined by Smith et al. (2006). In the Smith et al. study, paralaminae cells tended to not show bursting, similar to our preliminary observations in mouse thalamotectal cells (Patel et al., 2015b).

The current finding that a subset of cells from the BIC that project to the IC are GABAergic (Figs. 7, 8) is consistent with a body of literature from the visual system in mammals as well as nonmammalian auditory thalamotectal systems. For example, using an isolated frog brain preparation, Endepols and Walkowiak (1999, 2001) observed short latency IPSPs in the frog homolog of the IC using intracellular recordings after electrical stimulation of the thalamus. Similarly, Ponnath and Farris (2014) observed drops in acoustic responsiveness of frog IC neurons after thalamic stimulation. It should be noted that other interpretations of these data are possible. Electrical stimulation of the thalamus could trigger hyperpolarizing currents in the IC via collaterals of ascending tectothalamic inhibitory afferents, which would be antidromically activated after electrical stimulation. Although it is not known if such ascending GABAergic tectothalamic projections are present in the frog, they are found in both mammalian (Winer et al., 1996; Peruzzi et al., 1997; Venkataraman and Bartlett, 2013; Llano et al., 2014) and nonmammalian preparations (Ito and Atoji, 2016). In the visual system, an inhibitory projection from the pretectum to superior colliculus has been identified using both electrophysiological (Born and Schmidt, 2004) and anatomical (Appell and Behan, 1990; Kenigfest and Belekova, 2009) methods.

The current data, combined with previous findings of a combined excitatory/inhibitory set of projections from the IC to the MGB (Winer et al., 1996; Peruzzi et al., 1997; Venkataraman and Bartlett, 2013; Llano et al., 2014), and known inputs from the IC to the nucleus of the BIC (Kudo and Niimi, 1980) suggest that the IC and the nucleus of the BIC contain reciprocal mixed excitatory and inhibitory inputs. Given the strong projection from the AC to the nucleus of the BIC (Andersen et al., 1980; Saldaña et al., 1996; Mellott et al., 2014), and the finding that inactivation of the AC

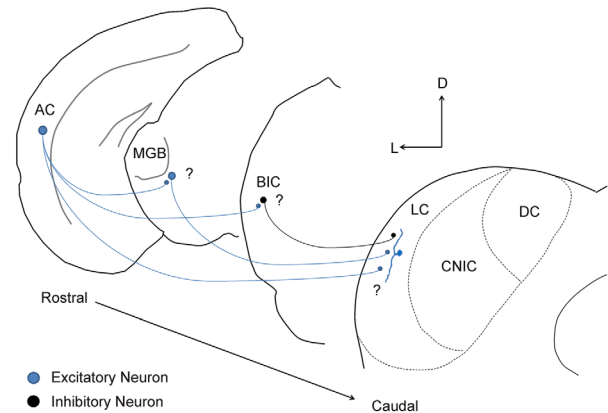


Figure 10. Hypothesized organizational scheme of descending projections to the IC. Neurons in the IC receive excitatory input from the AC and posterior thalamus (blue circles representing neurons) and GABAergic input from the BIC (black circles representing neurons). It is not yet known if IC-projecting neurons in the posterior thalamus and BIC receive direct input from corticothalamic axons (question marks) or if individual IC neurons receive both cortical and subcortical descending input. Although the diagram is focused on the LC for clarity, since both DC and LC receive substantial projections from AC and posterior thalamus, the hypothesized connective scheme could also be applied to the DC.

leads to disinhibition of some IC neurons (Jen et al., 2001; Anderson and Malmierca, 2013; Popeláø et al., 2015), the presence of an inhibitory projection from the BIC to the IC suggests that long-range corticocollicular inhibition may be mediated via GABAergic neurons in the BIC. The significance of the relative absence of GABAergic projections from the PP compared to BIC is not yet clear. Although both structures receive inputs from AC (Andersen et al., 1980; Arnault and Roger, 1990; Saldaña et al., 1996; Llano and Sherman, 2008; Mellott et al., 2014), PP also receives a diverse set of other inputs from hypothalamus and visceral brainstem nuclei (Chiba and Murata, 1985; Risold et al., 1994; Ruggiero et al., 1998), while BIC receives inputs from IC, brainstem auditory structures, and spinal cord nuclei (Kudo and Niimi, 1980; Flink et al., 1983; Aitkin and Phillips, 1984). It will be important in future studies to differentiate the input from these myriad brain regions onto GABAergic vs. non-GABAergic cells to help determine the functional implications of these findings.

A hypothesized organization of descending projections is shown in Figure 10. In this scheme, LC neurons (or DC neurons, which receive similar descending projections) receive descending projections from multiple sources: BIC, posterior thalamus, and AC. There are direct projections from the AC, and potentially indirect

projections from the thalamus and BIC, which contain a mixture of excitatory and inhibitory inputs. Multiple open questions remain. It is not yet known if IC-projecting neurons in the thalamus or BIC receive direct inputs from the AC (denoted as question marks in Fig. 10), nor is it known if individual neurons in the LC (or DC) integrate inputs from both the AC and thalamus/BIC or if these are segregated to different populations of midbrain neurons. Finally, projections from the AC to the IC emanate from two distinct laminar locations: a major projection from layer 5 and a smaller heterogeneous projection from the deepest regions of layer 6 (Schofield, 2009; Slater et al., 2013). The presence of multiple pathways emanating from the AC increases the number of potential combinations of descending circuit connections that can influence the IC. Therefore, physiological data about the corticocollicular system derived from manipulations of the AC should be interpreted in the context of potential polysynaptic pathways to the IC. This is particularly true in cases where cortical manipulation does not appear to have a major impact on certain IC response properties (Anderson and Malmierca, 2013), suggesting involvement of alternative pathways to achieve top-down modulation of the IC. Further work will be needed to explore these questions.

CONCLUSION

The data presented herein confirm previous results showing the distribution of IC-projecting cells in the BIC and paralamina thalamic nuclei, and extend them by establishing several new findings, including 1) the absence of traditional calcium-bindings in these cells; 2) the absence of branching of thalamotectal cells to forebrain structures associated with the medial MGB and paralamina structures; and 3) the finding that a subpopulation of IC-projecting cells in the BIC are GABAergic. These data suggest that cells projecting to the IC from thalamus and related structures comprise a unique class of evolutionarily conserved descending projections. The findings that descending projections from the AC have synapses (in some cases, very large synapses) in close physical proximity to regions containing thalamotectal cells (Llano and Sherman, 2008; Mellott et al., 2014), raise the possibility that at least some of the effects of cortical stimulation on IC response properties may be mediated polysynaptically, with a projection through the thalamus. This type of organization would suggest that the evolutionarily recently derived corticocollicular system is intrinsically linked to the more evolutionarily ancient thalamotectal system. Alternatively, the corticocollicular system may operate completely independently of the thalamotectal

system. Future studies will clarify the relationship between these two systems in modifying IC neuronal function.

ACKNOWLEDGMENTS

The authors thank Drs. Doug Oliver and Deborah Bishop from the University of Connecticut for generously providing us founder GAD-GFP mice and Dr. Yuchio Yanagawa for permission to use these mice. The authors also thank Junyu Li and Kate Srikant for their work on this project. We also thank the two anonymous reviewers whose suggestions greatly improved the article.

LITERATURE CITED

- Adams JC. 1980. Crossed and descending projections to the inferior colliculus. *Neurosci Lett* 19:1–5.
- Aitkin LM, Phillips SC. 1984. Is the inferior colliculus and obligatory relay in the cat auditory system? *Neurosci Lett* 44:259–264.
- Anderson L, Malmierca M. 2013. The effect of auditory cortex deactivation on stimulus-specific adaptation in the inferior colliculus of the rat. *Eur J Neurosci* 37:52–62.
- Andersen RA, Snyder RL, Merzenich MM. 1980. The topographic organization of corticocollicular projections from physiologically identified loci in the AI, All, and anterior auditory cortical fields of the cat. *J Comp Neurol* 191:179–494.
- Appell PP, Behan M. 1990. Sources of subcortical GABAergic projections to the superior colliculus in the cat. *J Comp Neurol* 302:143–158.
- Arnault P, Roger M. 1990. Ventral temporal cortex in the rat: connections of secondary auditory areas Te2 and Te3. *J Comp Neurol* 302:110–123.
- Bajo VM, King AJ. 2011. Cortical modulation of auditory processing in the midbrain. *Front Neural Circuits* 6:114–114.
- Bajo VM, Nodal FR, Bizley JK, Moore DR, King AJ. 2007. The ferret auditory cortex: descending projections to the inferior colliculus. *Cerebr Cortex* 17:475–491.
- Bordi F, LeDoux JE. 1994. Response properties of single units in areas of rat auditory thalamus that project to the amygdala II. Cells receiving convergent auditory and somatosensory inputs and cells antidromically activated by amygdala. *Exp Brain Res* 98:275–286.
- Born G, Schmidt M. 2004. Inhibition of superior colliculus neurons by a GABAergic input from the pretectal nuclear complex in the rat. *Eur J Neurosci* 20:3404–3412.
- Budinger E, Brosch M, Scheich H, Mylius J. 2013. The subcortical auditory structures in the Mongolian gerbil: II. Frequency-related topography of the connections with cortical field AI. *J Comp Neurol* 521:2772–2797.
- Chapman AM, Debski EA. 1995. Neuropeptide Y immunoreactivity of a projection from the lateral thalamic nucleus to the optic tectum of the leopard frog. *Vis Neurosci* 12:1–9.
- Chattopadhyaya B, Di Cristo G, Higashiyama H, Knott GW, Kuhlman SJ, Welker E, Huang ZJ. 2004. Experience and activity-dependent maturation of perisomatic GABAergic innervation in primary visual cortex during a postnatal critical period. *J Neurosci* 24:9598–9611.
- Chiba T, Murata Y. 1985. Afferent and efferent connections of the medial preoptic area in the rat: a WGA-HRP study. *Brain Res Bull* 14:261–272.
- Clugnet MC, LeDoux JE, Morrison SF. 1990. Unit responses evoked in the amygdala and striatum by electrical

- stimulation of the medial geniculate body. *J Neurosci* 10: 1055–1061.
- Comoli E, Das Neves Favaro P, Vautrelle N, Leriche M, Overton PG, Redgrave P. 2012. Segregated anatomical input to sub-regions of the rodent superior colliculus associated with approach and defense. *Front Neuroanat* 6:9.
- Cruikshank SJ, Killackey HP, Metherate R. 2001. Parvalbumin and calbindin are differentially distributed within primary and secondary subregions of the mouse auditory forebrain. *Neuroscience* 105:553–569.
- Edwards SB, Ginsburgh CL, Henkel CK, Stein BE. 1979. Sources of subcortical projections to the superior colliculus in the cat. *J Comp Neurol* 184:309–329.
- Endepols H, Walkowiak W. 1999. Influence of descending forebrain projections on processing of acoustic signals and audiomotor integration in the anuran midbrain. *Eur J Morphol* 37:182–184.
- Endepols H, Walkowiak W. 2001. Integration of ascending and descending inputs in the auditory midbrain of anurans. *J Comp Physiol A* 186:1119–1133.
- Endepols H, Feng AS, Gerhardt HC, Schul J, Walkowiak W. 2003. Roles of the auditory midbrain and thalamus in selective phonotaxis in female gray treefrogs (*Hyla versicolor*). *Behav Brain Res* 145:63–77.
- Feng AS, Lin W. 1991. Differential innervation patterns of three divisions of frog auditory midbrain (torus semicircularis). *J Comp Neurol* 306:613–630.
- Flink R, Wiberg M, Blomqvist A. 1983. The termination in the mesencephalon of fibres from the lateral cervical nucleus. An anatomical study in the cat. *Brain Res* 259: 11–20.
- Ingle D. 1973. Disinhibition of tectal neurons by pretectal lesions in the frog. *Science* 180:422–424.
- Ito T, Atoji Y. 2016. Tectothalamic inhibitory projection neurons in the avian torus semicircularis. *J Comp Neurol* 524:2604–2622.
- Jen P, Sun X, Chen Q. 2001. An electrophysiological study of neural pathways for corticofugally inhibited neurons in the central nucleus of the inferior colliculus of the big brown bat, *Eptesicus fuscus*. *Exp Brain Res* 137:292–302.
- Jones EG. 2001. The thalamic matrix and thalamocortical synchrony. *Trends Neurosci* 24:595–601.
- Kenigfest N, Belekova M. 2009. Evolutionary evaluation of reciprocity of connections in the turtle tectofugal visual system. *J Evol Biochem Physiol* 45:406–416.
- Kudo M, Niimi K. 1980. Ascending projections of the inferior colliculus in the cat: an autoradiographic study. *J Comp Neurol* 191:545–556.
- Kuwabara N. 2012. Neuroanatomical technique for studying long axonal projections in the central nervous system: combined axonal staining and pre-labeling in parasagittal gerbil brain slices. *Biotechn Histochem* 87:413–422.
- Kuwabara N, Zook JM. 2000. Geniculo-collicular descending projections in the gerbil. *Brain Res* 878:79–87.
- Li X, Tsurudome K, Matsumoto N. 2005. Postsynaptic potentials of tectal neurons evoked by electrical stimulation of the pretectal nuclei in bullfrogs (*Rana catesbeiana*). *Brain Res* 1052:40–46.
- Llano DA, Sherman SM. 2008. Evidence for nonreciprocal organization of the mouse auditory thalamocortical-corticothalamic projection systems. *J Comp Neurol* 507: 1209–1227.
- Llano DA, Slater BJ, Lesicko AM, Stebbings KA. 2014. An auditory colliculothalamocortical brain slice preparation in mouse. *J Neurophysiol* 111:197–207.
- Lu E, Llano D, Sherman S. 2009. Different distributions of calbindin and calretinin immunostaining across the medial and dorsal divisions of the mouse medial geniculate body. *Hear Res* 257:16–23.
- Ma X, Suga N. 2001. Corticofugal modulation of duration-tuned neurons in the midbrain auditory nucleus in bats. *Proc Natl Acad Sci U S A* 98:14060–14065.
- Malmierca MS, Cristaudo S, Pérez-González D, Covey E. 2009. Stimulus-specific adaptation in the inferior colliculus of the anesthetized rat. *J Neurosci* 29:5483–5493.
- Malone B, Semple M. 2001. Effects of auditory stimulus context on the representation of frequency in the gerbil inferior colliculus. *J Neurophysiol* 86:1113–1130.
- Mellott JG, Bickford ME, Schofield BR. 2014. Descending projections from auditory cortex to excitatory and inhibitory cells in the nucleus of the brachium of the inferior colliculus. *Front Syst Neurosci* 8.
- Metzger RR, Greene NT, Porter KK, Groh JM. 2006. Effects of reward and behavioral context on neural activity in the primate inferior colliculus. *J Neurosci* 26:7468–7476.
- Nevue A, Elde C, Perkel D, Portfors C. 2015. Dopaminergic inputs to the inferior colliculus. *Assoc Res Otolaryngol Meet PS-566*.
- Patel M, Lesicko AM, Yang L, Taha G, Llano DA. 2015a. Characterization of the auditory thalamotectal projection in mouse. *Assoc Res Otolaryngol Meet PS-574*.
- Patel MB, Sons S, Yang L, Taha GA, Lesicko AMH, Yudintsev G, Llano DA. 2015b. The thalamotectal system: An ancient projection for modulating the auditory midbrain. *Proc Meet Acoust* 25:010004.
- Peruzzi D, Bartlett E, Smith PH, Oliver DL. 1997. A monosynaptic GABAergic input from the inferior colliculus to the medial geniculate body in rat. *J Neurosci* 17:3766–3777.
- Ponnath A, Farris HE. 2014. Sound-by-sound thalamic stimulation modulates midbrain auditory excitability and relative binaural sensitivity in frogs. *Front Neural Circuits* 8.
- Popelář J, Šuta D, Lindovský J, Bureš Z, Pysanenko K, Chumak T, Syka J. 2015. Cooling of the auditory cortex modifies neuronal activity in the inferior colliculus in rats. *Hear Res* [Epub ahead of print].
- Risold P, Canteras N, Swanson L. 1994. Organization of projections from the anterior hypothalamic nucleus: a Phaseolus vulgaris-leucoagglutinin study in the rat. *J Comp Neurol* 348:1–40.
- Ruggiero DA, Anwar S, Kim J, Glickstein SB. 1998. Visceral afferent pathways to the thalamus and olfactory tubercle: behavioral implications. *Brain Res* 799:159–171.
- Saldaña E, Feliciano M, Mugnaini E. 1996. Distribution of descending projections from primary auditory neocortex to inferior colliculus mimics the topography of intracollicular projections. *J Comp Neurol* 371:15–40.
- Schofield BR. 2009. Projections to the inferior colliculus from layer VI cells of auditory cortex. *Neuroscience* 159:246–258.
- Senatorov V, Hu B. 2002. Extracortical descending projections to the rat inferior colliculus. *Neuroscience* 115:243–250.
- Slater BJ, Willis AM, Llano DA. 2013. Evidence for layer-specific differences in auditory corticocollicular neurons. *Neuroscience* 229:144–154.
- Smith PH, Bartlett EL, Kowalkowski A. 2006. Unique combination of anatomy and physiology in cells of the rat paralamina thalamic nuclei adjacent to the medial geniculate body. *J Comp Neurol* 496:314–334.
- Stebbins KA, Lesicko AM, Llano DA. 2014. The auditory corticocollicular system: molecular and circuit-level considerations. *Hear Res* 314:51–59.
- Suga N. 2008. Role of corticofugal feedback in hearing. *J Comp Physiol A* 194:169–183.

- Takada M, Itoh K, Yasui Y, Sugimoto T, Mizuno N. 1985. Topographical projections from the posterior thalamic regions to the striatum in the cat, with reference to possible tecto-thalamo-striatal connections. *Exp Brain Res* 60:385–396.
- Tamamaki N, Yanagawa Y, Tomioka R, Miyazaki JI, Obata K, Kaneko T. 2003. Green fluorescent protein expression and colocalization with calretinin, parvalbumin, and somatostatin in the GAD67-GFP knock-in mouse. *J Comp Neurol* 467:60–79.
- Torii M, Hackett TA, Rakic P, Levitt P, Polley DB. 2013. EphA signaling impacts development of topographic connectivity in auditory corticofugal systems. *Cerebr Cortex* 23:775–785.
- Trachtenberg M, Ingle D. 1974. Thalamo-tectal projections in the frog. *Brain Res* 79:419–430.
- Venkataraman Y, Bartlett EL. 2013. Postnatal development of synaptic properties of the GABAergic projection from the inferior colliculus to the auditory thalamus. *J Neurophysiol* 109:2866–2882.
- Winer JA, Saint Marie RL, Larue DT, Oliver DL. 1996. GABAergic feedforward projections from the inferior colliculus to the medial geniculate body. *Proc Natl Acad Sci U S A* 93:8005–8010.
- Winer JA, Larue DT, Diehl JJ, Hefti BJ. 1998. Auditory cortical projections to the cat inferior colliculus. *J Comp Neurol* 400:147–174.
- Winer JA, Kelly JB, Larue DT. 1999. Neural architecture of the rat medial geniculate body. *Hear Res* 130:19–41.
- Winer JA, Chernock ML, Larue DT, Cheung SW. 2002. Descending projections to the inferior colliculus from the posterior thalamus and the auditory cortex in rat, cat, and monkey. *Hear Res* 168:181–195.
- Yan J, Ehret G. 2001. Corticofugal reorganization of the mid-brain tonotopic map in mice. *Neuroreport* 12:3313–3316.
- Yan J, Ehret G. 2002. Corticofugal modulation of midbrain sound processing in the house mouse. *Eur J Neurosci* 16:119–128.
- Yan W, Suga N. 1998. Corticofugal modulation of the mid-brain frequency map in the bat auditory system. *Nat Neurosci* 1:54–58.
- Yan J, Zhang Y, Ehret G. 2005. Corticofugal shaping of frequency tuning curves in the central nucleus of the inferior colliculus of mice. *J Neurophysiol* 93:71–83.